Hindawi
International Journal of Chemical Engineering
Volume 2023, Article ID 9567708, 12 pages
https://doi.org/10.1155/2023/9567708

Research Article

Effects of Pyrrhotite on the Combustion Behavior and the Kinetic Mechanism of Pyrite-Pyrrhotite Mixture Powders in the Air

Changshun Tian,[1,2] **Yunzhang Rao**,[2,3] **Gang Su**,[3] **and Tao Huang**[3]

[1]*School of Resources and Architectural Engineering, Gannan University of Science and Technology, Ganzhou 341000, China*
[2]*Key Laboratory of Mining Engineering of Jiangxi Province, Jiangxi University of Science and Technology, Ganzhou 341000, China*
[3]*Faculty of Resources and Environmental Engineering, Jiangxi University of Science and Technology, Ganzhou 341000, China*

Correspondence should be addressed to Changshun Tian; 9320090329@jxust.edu.cn and Yunzhang Rao; raoyunzhang@jxust.edu.cn

Received 10 October 2022; Revised 28 November 2022; Accepted 6 December 2022; Published 28 June 2023

Academic Editor: Yanqing Niu

In this study, we performed a comparative analysis of the combustion behavior of pyrite, pyrrhotite, and pyrite-pyrrhotite mixture (mixed mineral) powders in an air atmosphere. To study the influence of the pyrrhotite content in mixed mineral powders on the combustion behavior in the air, thermogravimetric mass spectrometry, X-ray diffraction analysis, and scanning electron microscopy were employed. The results indicated that pyrrhotite lead to a weight gain in the mixed minerals during the combustion process. Pyrrhotite particles are more easily adsorbed on the surface of pyrite particles during mixed mineral combustion due to their strong ability to absorb oxygen, which accelerates pyrite combustion. The weight loss of mixed minerals decreased during the combustion process with increasing pyrrhotite content, resulting from pyrite encapsulation by agglomerated and sintered pyrrhotite during combustion. The calculated kinetic parameters and phase analysis results suggested that pyrite combustion is consistent with the shrinking core mechanism, and in the combustion process, the irregular pyrite particle shrank into a spherical particle; the combustion products of pyrrhotite grew in a layer-by-layer manner. Pyrrhotite combustion corresponded to the three-dimensional diffusion mechanism, and mixed mineral combustion was dominated by the shrinking core mechanism and supplemented by the three-dimensional diffusion mechanism. SO_2, as the main combustion product, was continuously generated and volatilized in the reaction, signifying that the combustion reaction of pyrite is a two-phase reaction involving gas and solid.

1. Introduction

Iron sulfide minerals play a key role in geochemistry, marine systems, oil storage and transportation, and environmental management [1–5]. As iron sulfide minerals, pyrite (FeS_2) is widely applied to sulfuric acid production, metallurgy, and other industries [6, 7], whereas pyrrhotite ($Fe_{1-x}S$) has practical application values in biomedicine, magnetic material manufacturing, water treatment, and battery processing, among other fields [8, 9]. However, large amounts of iron sulfide dust produced during iron sulfide mineral mining, storage, and transportation pose the risk of combustion and even explosion if dust explosion pentagon conditions are met [10, 11]. Moreover, pyrite and pyrrhotite, as minerals associated with coal and chalcopyrite, are among the main sources of sulfur dioxide emissions during the combustion of coal and chalcopyrite leaching, which is a significant cause of environmental pollution [12–14]. Accidents caused by combustion and explosion, as well as pollution in iron sulfide mines, have resulted in significant damage and loss of life in several countries in the past decades [15, 16]. Therefore, to address the challenges associated with the use of iron sulfide minerals, it is essential to study the phase transition behavior of iron sulfide combustion in an air atmosphere.

Pyrite combustion in the air is controlled by temperature and oxygen concentration, among other factors, and involves the transformation of two diverse forms [17]. Some

researchers have proposed that pyrite directly converts to hematite (Fe_2O_3; one-step direct oxidation theory) [18–25], while others have considered that pyrite first decomposes into porous pyrrhotite and that the porous pyrrhotite further oxidizes to other iron oxides (step-by-step theory) [17, 26–28]. Subject to temperature, one-step direct oxidation theory suggests that pyrite directly oxidizes to produce Fe_2O_3 at temperatures below 530°C, and sulfate formation occurs during the reaction [23]. The oxidation products of pyrite at 1200 and 1500°C are Fe_2O_3 and Fe_3O_4, respectively [19, 20]. However, according to step-by-step theory, pyrite first decomposes to form magnetic pyrite (pyrrhotite) at 610°C, followed by further oxidation of pyrrhotite, with the end products comprising FeS_2, $Fe_{1-x}S$, and Fe_2O_3/Fe_3O_4 [27]. In addition, some studies have demonstrated that pyrrhotite appears at low temperatures ($T < 270$°C), but pyrrhotite oxidizes to iron oxides at high temperatures [29]. Influenced by the concentration of oxygen, the one-step direct oxidation theory considers that Fe_2O_3 is the stabilized oxide in a hypoxic atmosphere at ~1327°C [18], and Fe_3O_4 is formed at high temperatures [19, 20]. Fe_3O_4 is the only stabilized product under high oxygen concentration conditions when the combustion temperature is above 1427°C, while Fe_2O_3 only exists at temperatures below 1227°C [17, 21]. According to the step-by-step theory, only pyrrhotite is formed in atmospheres of 100 ppm to 1009 ppm O_2 gas, in a temperature range of 484–538°C [26]. Thus, there is no consensus regarding the combustion process of pyrite, and this topic requires further research.

Pyrrhotite is generally studied as an intermediate product during pyrite combustion, but only few studies have been performed employing pyrrhotite as a reactant [30–35]. Özdeniz and Kelebek [30] found that pyrrhotite combustion occurs through a spontaneous self-heating reaction. Cruz et al. [31] suggested that the reactivity of pyrrhotite is controlled by the formation of an oxidation product layer, which can encapsulate and passivate the surface of pyrrhotite, and that the elemental S layer is dominant. Zhao et al. [32] revealed that O_2 exhibits greater adsorption energy on the pyrrhotite surface than on the pyrite surface. Dunn and Chamberlain [33] showed that the ignition temperature decreases with an increase in the pyrrhotite content. Alksnis et al. [34] prepared iron oxides and sulfur dioxide by roasting pyrrhotite. The optimum roasting conditions were estimated as follows: the gas flow rate was at least 200 mL/min, the temperature was 850°C, and the oxygen partial pressure was equal to that in the air. Luo et al. [8] proposed that the pyrrhotite combustion process occurs in four stages: oxidative decomposition of pyrrhotite, formation of ferric sulfate, decomposition of ferric sulfate, and formation of hematite. Moreover, Lv et al. [35] theorized that CO_2 participates in the entire oxidative decomposition process of pyrrhotite. Nevertheless, the studies on pyrrhotite combustion are relatively scarcer than those on pyrite combustion.

The combustion behavior of mixtures is more complex than that of single compounds, and therefore, associated studies are rather sparse. The experiments performed by Yang et al. [36] using a FeS-FeS_2 mixture in a nitrogen atmosphere revealed that the strength of surface adsorption and oxygen storage capacity of the FeS-FeS_2 mixture increase with the increasing mass fraction and fractal dimension of FeS, leading to spontaneous combustion of sulfide ore. Li et al. [37] studied the phase transition process of a FeS-FeS_2 mixture in a helium and H_2S atmosphere at high temperatures and found that the oxidation of sulfur is a prerequisite for the formation of pyrite. However, the combustion process and the mechanism in an air atmosphere remain unclear and necessitate further studies.

To explore the influence of the pyrrhotite content on the combustion of pyrite-pyrrhotite mixtures (mixed mineral), we used thermogravimetric mass spectrometry (TG–MS), X-ray diffraction (XRD) analysis, and scanning electron microscopy (SEM) in this study to determine solid and gaseous products. By calculating apparent activation energy, the associated chemical process and the kinetic mechanism, as well as the role of the pyrrhotite content in pyrite combustion, were determined. The study is aimed at providing a theoretical basis for the chemical reaction, revealing pyrrhotite participation in pyrite dust explosions, and the knowledge of which may help prevent pyrite mountain fires and explosion accidents in the future.

2. Materials and Methods

2.1. Materials and Characterization. Commercial pure pyrite and pyrrhotite (Guangzhou Huadu District Huadong Yeshi Stone Specimen Firm, Guangdong, China) were used to conduct the tests. After grinding, samples were sieved with a 200-mesh standard sieve (pore diameter = 75 μm), and the sieved pyrite and pyrrhotite were, respectively, mixed at mass ratios of 1 : 0.1, 1 : 0.25, 1 : 0.5, 1 : 0.75, 1 : 1, 1 : 1.25, 1 : 1.5, 1 : 1.75, and 1 : 2. The particle sizes and the surface structure of pyrite, pyrrhotite, and pyrite-pyrrhotite mixtures at a mass ratio of 1 : 1 (referred to as mixed minerals (1 : 1)) were studied using a laser diffraction analyzer (2000E, Jinan Winner, China) and SEM (MLA650F, FEI, USA), and the results of which are shown in Figure 1. The three minerals exhibit nonuniform particle sizes and irregularly shaped structures, and the majority of the mineral particles were <45 μm in size, with a median particle size of <33 μm. The results of the particle size analysis were in good agreement with the SEM analysis results. The moisture contents of ore samples were determined after drying at 80°C for 24 h in a constant-temperature drying oven, and the tested samples were almost free of moisture.

The compositions of the tested samples and combustion products were analyzed using XRD (Empyrean, PANalytical, Holland) at 27°C. The contents of Fe and S in the ore samples were determined using titration (implementing standards of GB/T 6730.65-2009 [38]) and the direct combustion-iodometric method (implementing standards of YS/T575.17-2007 [39]), respectively. The results showed that FeS_2 and monoclinic Fe_7S_8 are the main components in pyrite and pyrrhotite, respectively. The contents of Fe and S in pyrite were 45.74% and 58.23%, respectively, and those in pyrrhotite were 53.02% and 38.91%, respectively. The ratios of S to Fe in pyrite and pyrrhotite were 2.0285 and 1.1694, respectively, which were in good agreement with their

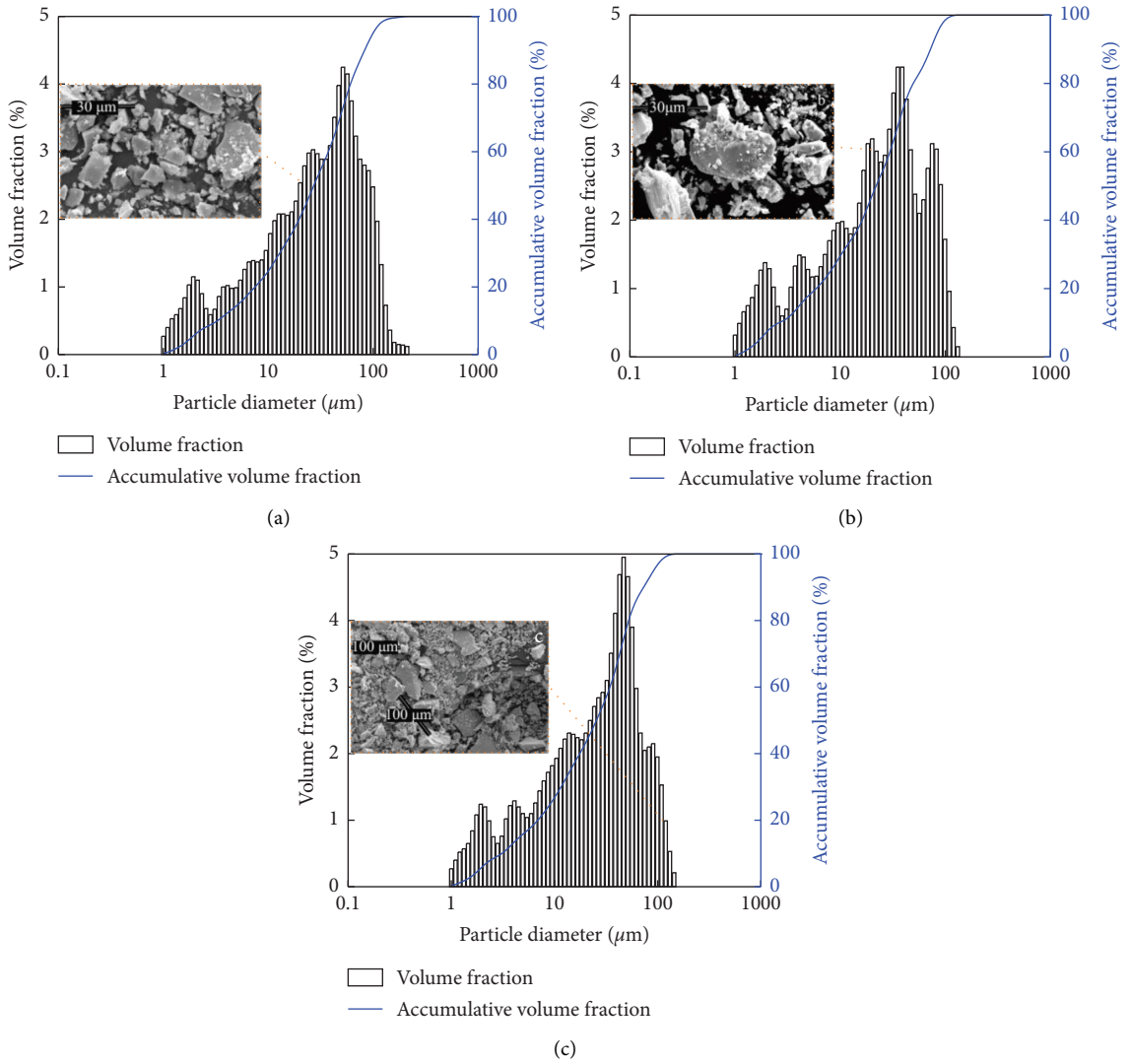

Figure 1: Particle size and the surface structure of ore dust. (a) Pyrite; (b) mixed minerals (1 : 1); (c) pyrrhotite.

stoichiometric values, and the measured results were consistent with the results of the XRD analysis.

2.2. Experimental Methods. The experimental procedure is shown in Figure 2. TG-MS (TA449F3–QMS403, NETZSCH, Germany) was used to estimate the weight loss and real-time gas products of pyrite, pyrrhotite, and mixed minerals (1 : 1). The airflow rate for the TG analysis was 50 mL/min, the nitrogen flow rate of MS was 20 mL/min, and the heating rate was 10°C/min. To study the influence of the pyrrhotite content on mixed mineral combustion, measurements were conducted using TG (Hitachi, STA7200, Japan) at the same airflow rate and heating rate as in TG-MS. The mass of each of the aforementioned test samples was 10 ± 0.5 mg.

Based on the results of the TG-MS test, the combustion test was performed at the differential scanning calorimetry (DSC) peak temperature in an electric box furnace (KSL–1200X–M, HF–Kejing, China) to study solid products. First, 2.5 g each of pyrite, pyrrhotite, and mixed minerals (1 : 1) was placed in a trapezoidal corundum crucible with dimensions of $80 \times 40 \times 17$ mm, where the airflow rate was set at 200 mL/min and the heating rate was 10°C/min. After achieving the test temperature and maintaining it at a constant value for 20 min, the samples were allowed to ventilate until the combustion products were cooled to room temperature in the box, and the products were then characterized using XRD and SEM.

3. Results and Discussion

3.1. Combustion Behavior of Iron Sulfide Minerals in an Air Atmosphere. The weight loss and real-time variation of oxygenated sulfide gas products of the three ore dust samples during combustion in the air are shown in Figure 3. The total weight loss of pyrite, mixed minerals (1 : 1), and pyrrhotite was 34.11%, 25.20%, and 18.38%, respectively.

Compared with the combustion of pyrrhotite and mixed minerals (1 : 1), pyrite combustion only involved four stages, and the second stage of the weight gain was not observed, as presented in Figure 3 and Table 1.

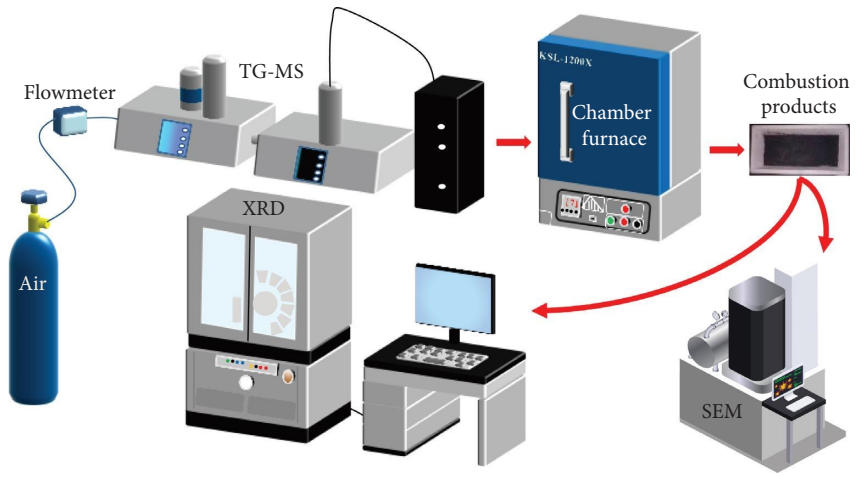

Figure 2: Schematic diagram of the experimental instrument and process.

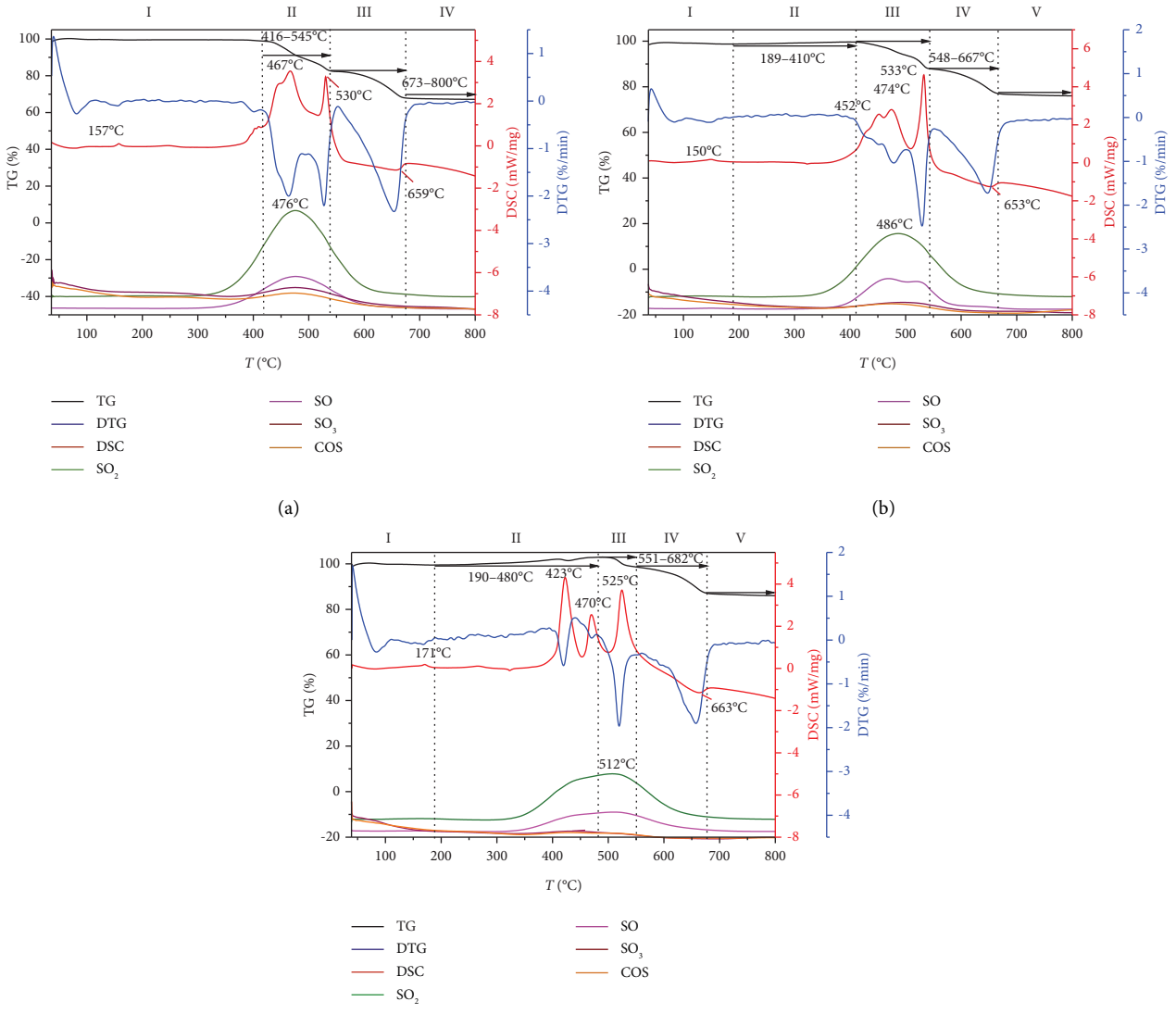

Figure 3: Combustion of the ore dust samples. (a) Pyrite; (b) mixed minerals (1 : 1); (c) pyrrhotite.

Table 1: Stage characteristics of the combustion reaction.

Sample type	Reaction stages	Temperature range/°C	Weight variation/%	Peak temperature of the DSC curve/°C
Pyrite	I	27–416	−0.99	157
	II	416–545	−15.58	467
	III	545–673	−16.69	530
	IV	673–800	−0.90	659
Mixed minerals (1 : 1)	I	27–189	−1.02	150
	II	189–410	+0.79	452
	III	410–548	−11.33	474
	IV	548–667	−11.16	533
	V	667–800	−2.48	653
Pyrrhotite	I	27–190	−0.94	171
	II	190–480	+3.24	423
	III	480–551	−4.36	470
	IV	551–682	−12.70	525
	V	682–800	−0.62	663

In the first stage, pyrite, mixed minerals, and pyrrhotite exhibited lower weight losses than they did in the other stages, and short exothermic peaks on the DSC curve appeared at 157, 150, and 171°C. Considering the elemental analysis results in Section 2.1, namely, the presence of excess S monomers, and S melts at ~112.8°C, we assume that the peak is generated due to the reaction of S with O_2 to form SO_2. Hence, an increase in the SO_2 curve can also confirm this result.

In the second stage, pyrite underwent a weight loss of 15.58%. Elemental sulfur on the surface of pyrite particles volatilized [40] and reacted with O_2 to form SO_2, with SO_2 production being maximum at ~476°C. Notably, small amounts of SO, SO_3, and COS were simultaneously observed, which is consistent with the results of the studies by Jorgensen and Moyle [23] and Lv et al. [35], wherein SO and COS were detected, respectively. However, the weights of pyrrhotite and mixed minerals increased by 3.24% and 0.79%, respectively, which is associated with the formation of $FeSO_4$ and Fe_2O_3 from oxidative decomposition of pyrrhotite [8, 41]. Additionally, a large amount of gaseous SO_3 was formed.

In the third stage, the weight loss of pyrite was 16.69%. An endothermic peak was observed at 659.3°C on the DSC curves. Hu et al. [17] reported that sulfate would be formed at approximately 600–650°C, and the endothermic peak was a result of sulfate decomposition, which was verified by analyzing solid-phase products. Pyrrhotite showed a weight loss of 4.36%, which is related to the emission of S due to pyrrhotite decomposition at ~550°C [8, 42]. S, released during combustion, reacted with O_2 to form SO, SO_2, SO_3, and COS, and the amount of SO_2 produced was maximum at ~512°C. The weight loss of mixed minerals was 11.33%, which may be due to the gasification of S originating from original pyrrhotite [41] and pyrrhotite formed through pyrite pyrolysis [40].

In the fourth stage, the weight loss of pyrite was only 0.90%, and it continued above 800°C. Furthermore, the weight losses of pyrrhotite and mixed minerals were 12.70% and 11.16%, respectively, resulting from further pyrolysis of $FeSO_4$ formed via pyrrhotite decomposition to release SO_2 in the temperature range of 600–900°C [8]. Moreover, an endothermic peak was detected at 663.4°C, due to the decomposition of the molten material $[Fe_2(SO_4)_3]_2{\cdot}Fe_2O_3$ [43].

In the fifth stage, the weight losses of pyrrhotite and mixed minerals had low values of 0.62% and 2.48%, respectively, and they continued at 800°C. Furthermore, the slope of the TG curve was very small, indicating that the combustion reaction was essentially completed at that time.

3.2. Influence of the Pyrrhotite Content on the Combustion of Pyrite-Pyrrhotite Mixtures. The effect of the pyrrhotite content on the combustion of pyrite-pyrrhotite mixtures in an air atmosphere is shown in Figure 4. The first peak temperature on the DTG curve generally increased with an increase in the pyrrhotite content (except for a few points, e.g., the mass ratio 1 : 0.1), which may be due to the fact that pyrrhotite contains more amount of sulfur and takes longer to completely combust than pyrite does. The second peak temperature on the DTG curve decreased with an increase in the pyrrhotite content because pyrrhotite is easier to oxidize [44]. With an increase in the pyrrhotite content, the amounts of $FeSO_4$ and Fe_2O_3 formed via decomposition increased and the reaction rate increased. Although the two peak temperatures fluctuated, there was no variation in the third and fourth peak temperatures on the DTG curve with an increase in the pyrrhotite content, which indicated that pyrrhotite mainly influenced the initial and weight gain stages of combustion of the pyrite-pyrrhotite mixture.

Moreover, the weight loss rate of mixed ore evidently decreased with an increase in the pyrrhotite content, which indicated that the combustion of pyrite is more violent than that of pyrrhotite in the air, and pyrite combusted with more gas volatilized, as shown in Figure 4. This phenomenon has also been observed in explosion experiments [45].

3.3. Characteristics of Solid Products from Iron Sulfide Minerals Combustion. The combustion products of the three samples in the air were characterized using XRD at room temperature (27°C), the peak temperature on the DSC curve, and the final test temperature (800°C), and the results are

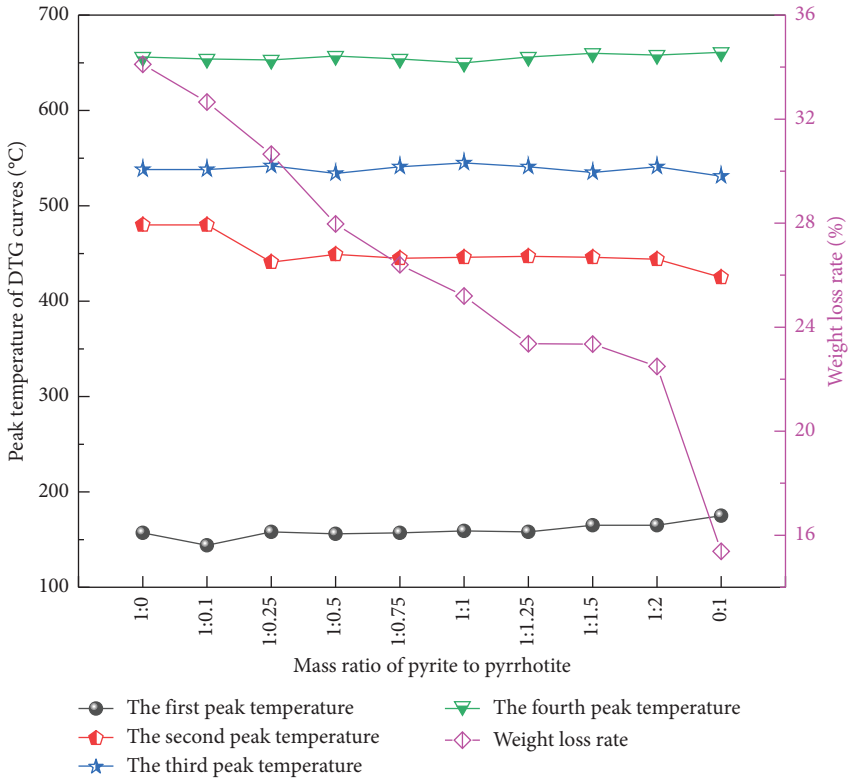

Figure 4: Relationship between the pyrrhotite content and the peak heat loss and the weight loss rate.

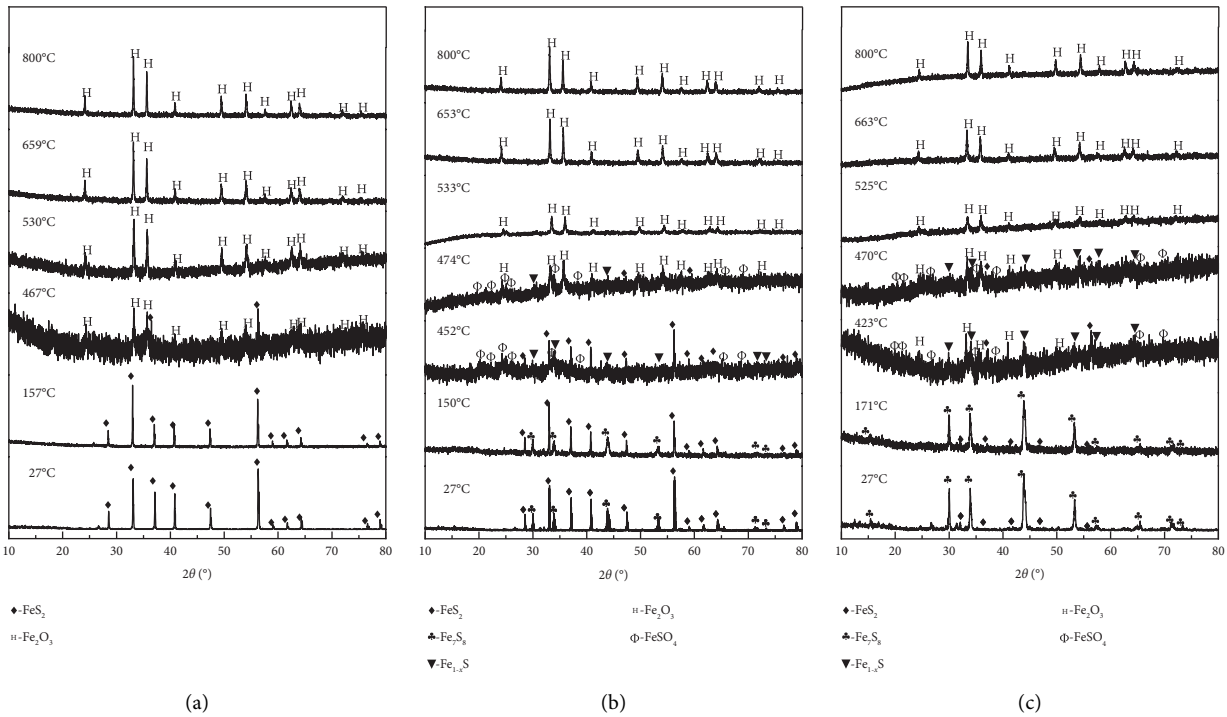

Figure 5: XRD analysis results of combustion products. (a) Pyrite; (b) mixed minerals (1 : 1); (c) pyrrhotite.

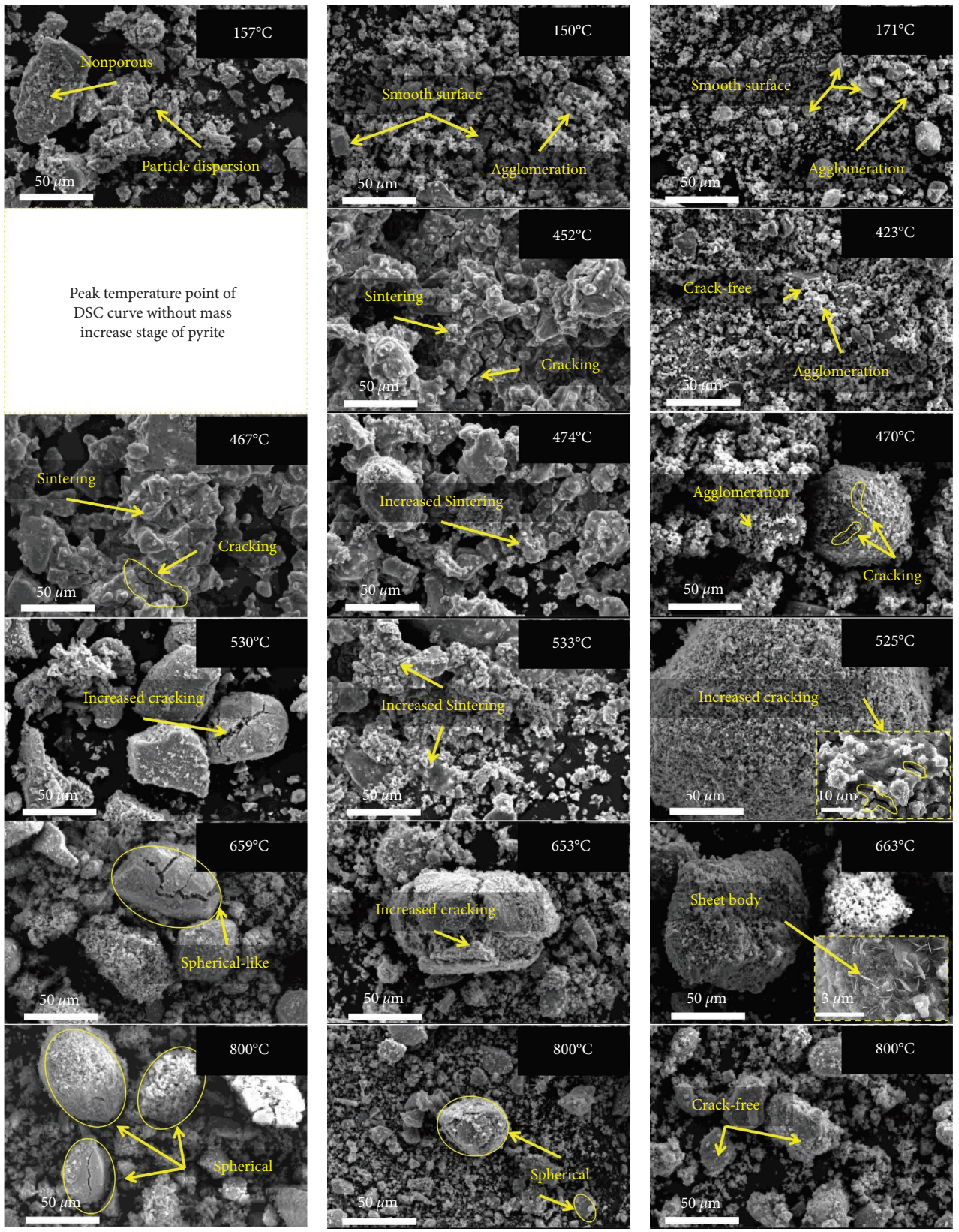

(a) (b) (c)

Figure 6: SEM analysis results of combustion products at different temperatures. (a) Pyrite; (b) mixed minerals (1 : 1); (c) pyrrhotite.

shown in Figure 5. Surface morphology changes in combustion products are shown in Figure 6.

As shown in Figures 5(a) and 6(a), at 157°C, dispersed pyrite particles with smaller sizes were adsorbed on the surface of large particles, which are dense and nonporous. No phase change was observed at that time, indicating that the weight loss is caused by S volatilization. The phase change in pyrite occurred at 467°C, and hematite was formed, which is consistent with the experimental results reported by Aracena et al. [22], Jorgensen and Moyal [23], and Schorr and Everhart [25]. At 467°C, as small particles were sintered, some cracks developed on the surface of large particles, and the gas volatilized from cracks. At 530°C, the surface of large particles became smoother and cracks became larger, and all pyrite was consumed and converted to Fe_2O_3. At 659°C, the particles gradually shrank and tended to be ellipsoidal in shape. Compared with the particles at 530°C, the cracking degree on the surface of single particles increased, and fine particles were more agglomerated. However, intermediate sulfate was not detected at this time. Jorgensen and Moyal [46] suspected that the XRD analysis conducted for distinguishing adjacent phases through diffraction peaks had errors. At 800°C, both sintered particles and large particles possessed an ellipsoidal structure and the combustion products were Fe_2O_3, which is the same as at 530°C. Pyrrhotite, the intermediate product described in [26, 27, 47], was not found in the results of the XRD analysis. FeO, the final product described in [48], was also not detected. Combined with the analysis results of the gas-phase products in Section 3.1, the chemical reaction equation of pyrite combustion in the air is shown in the equation as follows:

$$2FeS_2(s) + \left(2x + \frac{3}{2}\right)O_2(g) = Fe_2O_3(s) + 4SO_x(g). \quad (1)$$

At 423°C, the phase of pyrrhotite began to change, and as the temperature increased from 423°C to 800°C, the crystalline phase of Fe_2O_3 gradually stabilized, as shown in Figure 5(c). Additionally, $FeSO_4$ was detected at 423°C and 470°C, confirming that the weight gain stage was caused by the production of Fe_2O_3 and $FeSO_4$, which was consistent with the result reported in [8]. Meanwhile, the yield of SO, SO_2, and SO_3 increased, especially that of SO_3, which was maximum at 435.1°C, as shown in Equation (2). Notably, the phase of pyrrhotite changed from monoclinic Fe_7S_8 to hexagonal $Fe_{1-x}S$ at 423°C and 470°C, which was consistent with the pyrolysis phenomenon in a N_2 atmosphere [49]. The reaction is shown in Equation (3). Small particles were adsorbed on large particles with a smooth surface and underwent sintering and cracking and formation of a dense sintered body at 171°C, 423°C, and 470°C, respectively, as shown in Figure 5(c). In addition, Fe_3O_4 and $[Fe_2(SO_4)_3]_2{\cdot}Fe_2O_3$ originating from the oxidation of pyrrhotite at 425–520°C and 663.4°C, respectively, were not found [43]. Moreover, $Fe_{1-x}S$ and $FeSO_4$ were converted to Fe_2O_3, resulting in the formation of a large amount of SO_2 and SO_3 at 470–525°C, which occurred before obtaining the reaction temperature in [43]. The reaction equations are shown in Equations (4) and (5). The occurrence of different phases may be related to the heating rate [50, 51]. The cracking phenomenon was more apparent at 525°C than at 470°C, indicating that the degree of reaction at 525°C was higher than that at 470°C and that the maximum amount of gaseous products was produced at that temperature. It further demonstrates that the amount of gas products generated is related to the cracking degree and that the output of gas products increases with an increase in the extent of cracking. At 663°C, a new material with a thin crystal structure was produced. Considering the XRD analysis results, it is conjectured that the new material is sulfate formed via the thermal decomposition of the molten material $[Fe_2(SO_4)_3]_2{\cdot}Fe_2O_3$. The surface structure of pyrrhotite at 800°C was almost the same as that at 663°C. Compared with the case of pyrite, no cracking phenomenon was observed, indicating that the oxidation combustion mechanisms of pyrrhotite and pyrite are different. In summary, from the analysis results of gas-phase products, the chemical reaction equation of pyrrhotite combustion in the air can be simplified to Equation (6) without considering the intermediate process:

$$6Fe_{1-x}S(s) + (11-5x)O_2(g) = (2-2x)FeSO_4 + (2-2x)Fe_2O_3(s) + (4+2x)SO_2(g), \quad (2)$$

$$(1-x)Fe_7S_8(s) = 7Fe_{1-x}S(s) + (0.5-4x)S_2(g), \quad (3)$$

$$4Fe_{1-x}S(s) + (7-3x)O_2(g) = (2-2x)Fe_2O_3(s) + 4SO_2(g), \quad (4)$$

$$4FeSO_4(s) + O_2(g) = 2Fe_2O_3(s) + 4SO_3(g), \quad (5)$$

$$4Fe_{1-x}S(s) + (3-x)O_2(g) = (2-2x)Fe_2O_3(s) + 4SO_x(g). \quad (6)$$

However, the phase transformation of mixed minerals occurred at 452°C. At 452°C and 474°C, the phase transformation of mixed minerals was similar to that of pyrrhotite, and the combustion products contained $Fe_{1-x}S$, FeS_2, Fe_2O_3, and $FeSO_4$, which were responsible for line patterns, as shown in Figure 3(b), similar to those in Figure 3(c). Moreover, mixed minerals gained weight at 410°C, while pyrrhotite gained weight at 480°C, as shown in

Table 2: Calculated *Ea* values of three kinds of ore samples in different stages of combustion.

Sample type	Reaction stages	Function name	Mechanism	*Ea*/kJ·mol^{-1}
Pyrite	I	Third order	Chemical reaction, F_3, deceleration type *a-t* curve	1.42
	II	Avrami–Erofeev equation	Random nucleation and subsequent growth ($n = 4$)	194.81
	III	Reaction order	$n = 4$	8.04
	IV	Reaction order	$n = 4$	12.18
Mixed minerals (1 : 1)	I	Third order	Chemical reaction, F_3, deceleration type *a-t* curve	1.04
	II	Two-third order	Chemical reaction	4.55
	III	Avrami–Erofeev equation	Random nucleation and subsequent growth ($n = 3$)	105.79
	IV	Reaction order	$n = 4$	7.29
	V	Reaction order	$n = 4$	12.08
Pyrrhotite	I	Third order	Chemical reaction, F_3, deceleration type *a-t* curve	1.04
	II	Two-third order	Chemical reaction	5.28
	III	Two-third order	Chemical reaction	4.26
	IV	Inverse Jander equation	Three-dimensional diffusion	109.68

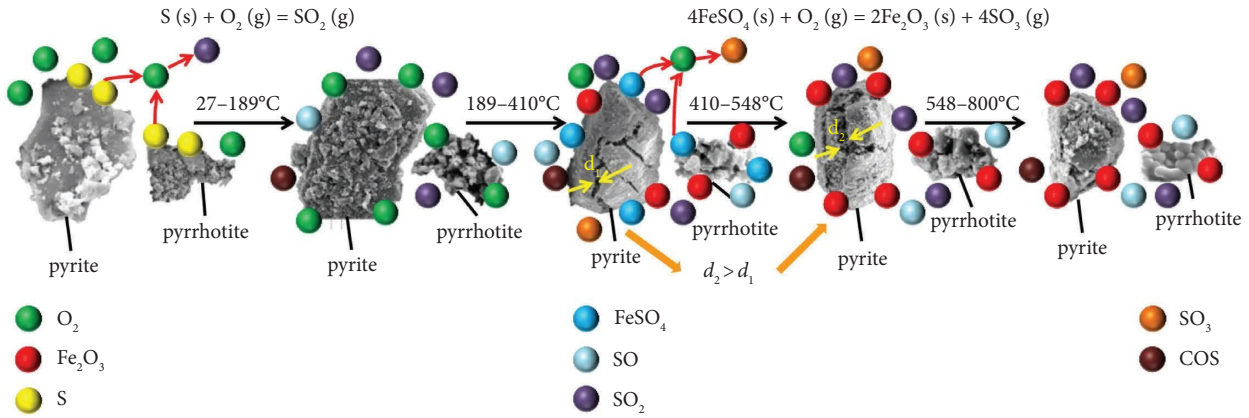

Figure 7: Combustion reaction process of the pyrite-pyrrhotite mixture.

Figures 3(b) and 3(c). It was confirmed that the weight gain is caused by the formation of Fe_2O_3 and $FeSO_4$, indicating that the addition of pyrrhotite promoted the formation of Fe_2O_3 and $FeSO_4$ in the pyrite-pyrrhotite mixture, which accelerated the reaction process in the weight gain stage. When the temperature exceeded 525°C, all the mixed minerals reacted to form Fe_2O_3, indicating that the conversion of both pyrrhotite and pyrite was complete. Kennedy and Sturman [43] found that pyrite FeS_2 formed in the oxidation of pyrrhotite and theorized that pyrite FeS_2 did not participate in the oxidation of $Fe_{1-x}S$. Therefore, considering the formation of gas-phase products, we theorized that the combustion of the pyrite and pyrrhotite mixture in the air occurs independently, with the chemical reaction equations shown in Equations (1) and (6). Upon analyzing the particle surface structure of the combustion products of mixed minerals (1 : 1), the products were similar to pyrite combustion products, as shown in Figure 6(b). Therefore, it may be considered that the interaction between minerals may be significantly influenced by the pyrite composition.

3.4. Analysis of the Combustion Kinetic Mechanism of Iron Sulfide Minerals. The apparent activation energy (*Ea*) can be used to describe the thermodynamic mechanism of nonisothermal and heterogeneous reaction systems [52]. Using the Coats–Redfern method, *Ea* of pyrite, mixed minerals (1 : 1), and pyrrhotite during the combustion process was calculated as follows:

$$\ln\left[\frac{g(a)}{T^2}\right] = \ln\left(\frac{AR}{\beta Ea}\right) - \frac{Ea}{RT}. \quad (7)$$

Herein, β is the heating rate (°C/min), A is the pre-exponential factor (min^{-1}), Ea is the apparent activation energy of the reaction (kJ/mol), R is the universal gas constant (8.314 J·K^{-1}·mol^{-1}), T is the absolute temperature (K), $g(a)$ is the integral function of the reaction model, and a is the decomposition conversion rate of three kinds of ore samples (%). $a = (m_0 - m_t)/(m_0 - m_\infty)$, where m_0 is the initial mass of the samples, m_t is the mass of the samples at time t, and m_∞ is the final mass of the samples.

We plotted the curve of $g(a)/T^2 - (1/T)$ based on the integral function and calculated *Ea* and *A* from the slope of the curve and intercept, respectively. *Ea* of the three ore samples in different reaction stages are listed in Table 2. In the rapid reaction stage, the *Ea* values of pyrite, mixed minerals (1 : 1), and pyrrhotite were 194.81, 105.79, and 109.68 kJ/mol, respectively. The *Ea* value of mixed minerals (1 : 1) was the smallest, indicating that the addition of

pyrrhotite facilitated the oxidation combustion reaction of pyrite, which is in agreement with the test results. Additionally, the mechanism analysis demonstrated that the presence of pyrrhotite, which led to a lower reaction order and lower reaction intensity of mixed minerals than those of pyrite, is the reason for the lower weight loss of mixed minerals than that of pyrite.

Based on the previously discussed kinetic mechanism analysis and phase analysis results of combustion products, the combustion process of the pyrite-pyrrhotite mixture in the air was dominated by pyrite and accompanied by the surface heterogeneous combustion of pyrrhotite [53, 54], as shown in Figure 7. Pyrrhotite particles were more easily adsorbed on the surface of pyrite particles during mixed mineral combustion due to their strong ability to absorb oxygen [44], which accelerated pyrite combustion. The reaction mechanism in the main combustion stage of mixed minerals was the same as that of pyrite. However, the weight loss rate of mixed minerals was higher than that of pyrrhotite due to the influence of pyrite composition. In the initial stage of combustion, S adsorbed in mixed minerals volatilized with the increasing temperature and reacted with O_2 to form SO_2. When the temperature increased to 410°C, cracks appeared on the surface of pyrite and pyrrhotite sintered to form Fe_2O_3 and $FeSO_4$. At 410–548°C, the cracks on the surface of pyrite became wider and $FeSO_4$ reacted with O_2 to form Fe_2O_3 and gaseous SO_3. When the temperature exceeded 548°C, only one kind of product was obtained, namely, Fe_2O_3. During this process, the irregular pyrite particle shrank into a spherical particle through the kinetic mechanism of random nucleation, which indicated that pyrite combustion conforms to the shrinking nucleation model [52]. Furthermore, the combustion products of pyrrhotite grew in a layer-by-layer manner, which indicated that the pyrrhotite combustion conforms to the three-dimensional diffusion model. During the entire reaction process, an amount of SO_2 and traces of other gases, such as SO, SO_3, and COS, were constantly generated and consumed, signifying that the combustion reaction of pyrite was a two-phase reaction involving gas and solid.

4. Conclusion

In this study, the combustion process and the kinetic mechanism of two typical iron sulfide minerals in the air were analyzed and the influence of the pyrrhotite content on the combustion of the pyrite-pyrrhotite mixture was investigated. The conclusions drawn were as follows:

(1) With the addition of pyrrhotite, the combustion process of the mixed ore became more complex, and mixed minerals and pyrrhotite underwent a weight gain stage during the combustion process compared with pyrite, due to the formation of Fe_2O_3 and sulfate $FeSO_4$. In the weight gain stage, the weight of pyrrhotite and mixed minerals increased by 3.24% and 0.79%, respectively.

(2) Pyrrhotite mainly affected the weight gain stage of mixed minerals. During that stage, the peak temperature of the DTG curve decreased with an increase in the pyrrhotite content, from 480°C to 425°C, which promoted the formation of $FeSO_4$. Owing to agglomeration and sintering of pyrrhotite, the weight loss rate of mixed minerals decreased with an increase in the pyrrhotite content. The weight loss of pyrrhotite was 18.73% less than that of pyrite.

(3) Combustion of iron sulfide minerals was a surface heterogeneous reaction involving gas and solid phases, which was controlled by the kinetic model. During the main combustion stage, the kinetic mechanism of pyrite was random nucleation, which accorded with the shrinking nucleation model, whereas that of pyrrhotite accorded with the three-dimensional diffusion model. The combustion process of mixed minerals was significantly influenced by pyrite, and the main reaction stage was the same as that of pyrite, which accorded with the random nucleation mechanism. At that time, pyrrhotite showed a three-dimensional diffusion trend.

(4) Although the chemical reaction equations and conversion kinetics of powder combustion of iron sulfide minerals were established, the analysis of the chemical reaction process was greatly influenced by the characterization methods used. Thus, there might be differences between the theoretical results and the actual continuous reaction process. To address this, the testing methods could be modified. A series of experiments in new in-situ devices with thermocouples and sensors could be used to study the intermediate reaction process.

Data Availability

The data used to support the findings of this study are included within the article.

Conflicts of Interest

The authors declare that they have no conflicts of interest.

Acknowledgments

This work was supported by the National Natural Science Foundation of China (NSFC) (51874149 and 51364010).

References

[1] R. C. Zhong, Y. Deng, W. B. Li et al., "Revealing the multi-stage ore-forming history of a mineral deposit using pyrite geochemistry and machine learning-based data interpretation," *Ore Geology Reviews*, vol. 133, Article ID 104079, 2021.

[2] Q. Zuo, Y. Xu, B. Yu et al., "NanoSIMS sulfur isotope studies of pyrite from the Early Paleozoic marine shale: implications for the sedimentary environment," *Marine and Petroleum Geology*, vol. 124, Article ID 104802, 2021.

[3] T. Wu, Z. J. Pan, B. Liu, L. D. Connell, R. Sander, and X. F. Fu, "Laboratory characterization of shale oil storage behavior: a comprehensive review," *Energy and Fuels*, vol. 35, no. 9, pp. 7305–7318, 2021.

[4] X. G. Lang, W. B. Tang, H. R. Ma, and B. Shen, "Local environmental variation obscures the interpretation of pyrite

sulfur isotope records," *Earth and Planetary Science Letters*, vol. 533, Article ID 116056, 2020.

[5] J. C. Gao, H. B. Sui, S. Y. Wu et al., "Interaction study of oxygen and iron-sulfur clusters based on the density functional theory," *International Journal of Chemical Engineering*, vol. 2022, Article ID 9812188, 9 pages, 2022.

[6] Q. Q. Huang and R. Honaker, "Recent trends in rock dust modifications for improved dispersion and coal dust explosion mitigation," *Journal of Loss Prevention in the Process Industries*, vol. 41, pp. 121–128, 2016.

[7] Q. Z. Li, Q. L. Tao, C. C. Yuan, Y. N. Zheng, G. Y. Zhang, and J. F. Liu, "Investigation on the structure evolution of pre and post explosion of coal dust using X-ray diffraction," *International Journal of Heat and Mass Transfer*, vol. 120, pp. 1162–1172, 2018.

[8] B. Luo, T. J. Peng, and H. J. Sun, "Innovative methodology for sulfur release from copper tailings by the oxidation roasting process," *Journal of Chemistry*, vol. 2020, Article ID 9812188, 11 pages, 2020.

[9] A. Yadollahi, H. Abdollahi, F. D. Ardejani, M. Mirmohammadi, and S. Magdouli, "Bio-oxidation behavior of pyrite, marcasite, pyrrhotite, and arsenopyrite by sulfur- and iron-oxidizing acidophiles," *Bioresource Technology Reports*, vol. 15, Article ID 100699, 2021.

[10] R. Walker, A. D. Steele, and D. T. B. Morgan, "Pyrophoric nature of iron sulfides," *Industrial & Engineering Chemistry Research*, vol. 35, no. 5, pp. 1747–1752, 1996.

[11] Y. Yanqiu and F. Jianchun, "Research on explosion characteristics of sulfur dust and risk control of the explosion," *Procedia Engineering*, vol. 84, pp. 449–459, 2014.

[12] F. Huang, L. Q. Zhang, B. J. Yi, Z. J. Xia, and C. G. Zheng, "Transformation pathway of excluded mineral pyrite decomposition in CO_2 atmosphere," *Fuel Processing Technology*, vol. 138, pp. 814–824, 2015.

[13] M. Sokić, B. Marković, S. Stanković et al., "Kinetics of chalcopyrite leaching by hydrogen peroxide in sulfuric acid," *Metals*, vol. 9, no. 11, 2019.

[14] E. Leiva, M. Cayazzo, L. Dávila, M. Torres, and C. Ledezma, "Acid mine drainage dynamics from a paste tailing deposit: effect of sulfate content on the consistency and chemical stability after storage," *Metals*, vol. 11, no. 6, 2021.

[15] Y. Z. Rao, C. S. Tian, W. Xu, C. Y. Xiao, B. Y. Yuan, and Y. Yu, "Explosion pressure and minimum explosible concentration properties of metal sulfide ore dust clouds," *Journal of Chemistry*, vol. 2020, Article ID 7980403, 12 pages, 2020.

[16] P. Chen, F. Yang, X. Qian et al., "Effect of sulfur content in sulfate-rich copper tailings on the properties of MgO-activated slag materials," *Materials*, vol. 15, no. 12, 2022.

[17] G. L. Hu, K. Dam-Johansen, S. Wedel, and J. P. Hansen, "Decomposition and oxidation of pyrite," *Progress in Energy and Combustion Science*, vol. 32, no. 3, pp. 295–314, 2006.

[18] L. S. Darken and R. W. Gurry, "The system iron-oxygen. II. equilibrium and thermodynamics of liquid oxide and other phases," *Journal of the American Chemical Society*, vol. 68, no. 5, pp. 798–816, 1946.

[19] O. C. Kopp and P. F. Kerr, "Differential thermal analysis of pyrite and marcasite," *American Mineralogist*, vol. 43, no. 11–12, pp. 1079–1097, 1958.

[20] J. P. Hansen, L. S. Jensen, S. Wedel, and K. Dam-Johansen, "Decomposition and oxidation of pyrite in a fixed-bed reactor," *Industrial & Engineering Chemistry Research*, vol. 42, no. 19, pp. 4290–4295, 2003.

[21] C. Toro, S. Torres, V. Parra et al., "On the detection of spectral emissions of iron oxides in combustion experiments of pyrite concentrates," *Sensors*, vol. 20, no. 5, 2020.

[22] A. Aracena, O. Jerez, R. Ortiz, and J. Morales, "Pyrite oxidation kinetics in an oxygen–nitrogen atmosphere at temperatures from 400 to 500 °C," *Canadian Metallurgical Quarterly*, vol. 55, no. 2, pp. 195–201, 2016.

[23] F. R. A. Jorgensen and F. J. Moyle, "Phases formed during the thermal analysis of pyrite in air," *Journal of Thermal Analysis*, vol. 25, no. 2, pp. 473–485, 1982.

[24] J. G. Dunn, G. C. De, and B. H. O'Connor, "The effect of experimental variables on the mechanism of the oxidation of pyrite," *Thermochimica Acta*, vol. 145, pp. 115–130, 1989.

[25] J. R. Schorr and J. O. Everhart, "Thermal behavior of pyrite and its relation to carbon and sulfur oxidation in clays," *Journal of the American Ceramic Society*, vol. 52, no. 7, pp. 351–354, 1969.

[26] Y. Hong and B. Fegley, "The kinetics and mechanism of pyrite thermal decomposition," *Berichte der Bunsen-Gesellschaft für Physikalische Chemie*, vol. 101, no. 12, pp. 1870–1881, 1997.

[27] A. Prasad, R. M. Singru, and A. K. Biswas, "Study of the roasting of pyrite minerals by Mössbauer spectroscopy," *Physica Status Solidi (a)*, vol. 87, no. 1, pp. 267–271, 1985.

[28] M. Vázquez, I. Moreno-Ventas, I. Raposo, A. Palma, and M. J. Díaz, "Kinetic of pyrite thermal degradation under oxidative environment," *Journal of Thermal Analysis and Calorimetry*, vol. 141, no. 3, pp. 1157–1163, 2020.

[29] A. Mitovski, N. Štrbac, D. Manasijević et al., "Thermal analysis and kinetics of the chalcopyrite-pyrite concentrate oxidation process," *Metalurgija*, vol. 54, no. 2, pp. 311–314, 2015.

[30] A. H. Özdeniz and S. Kelebek, "A study of self-heating characteristics of a pyrrhotite-rich sulphide ore stockpile," *International Journal of Mining Science and Technology*, vol. 23, no. 3, pp. 381–386, 2013.

[31] R. Cruz, I. González, and M. Monroy, "Electrochemical characterization of pyrrhotite reactivity under simulated weathering conditions," *Applied Geochemistry*, vol. 20, no. 1, pp. 109–121, 2005.

[32] C. H. Zhao, J. H. Chen, Y. Q. Li, Y. Chen, and W. Z. Li, "First-principle calculations of interaction of O_2 with pyrite, marcasite and pyrrhotite surfaces," *Transactions of Nonferrous Metals Society of China*, vol. 26, no. 2, pp. 519–526, 2016.

[33] J. G. Dunn and A. C. Chamberlain, "The effect of stoichiometry on the ignition behaviour of synthetic pyrrhotites," *Journal of Thermal Analysis*, vol. 37, no. 6, pp. 1329–1346, 1991.

[34] A. Alksnis, B. Li, R. Elliott, and M. Barati, "Kinetics of oxidation of pyrrhotite," in *Extraction. The Minerals, Metals & Materials Series*, pp. 403–413, Springer, Berlin, Germany, 2018.

[35] W. Z. Lv, D. X. Yu, J. Q. Wu, X. Yu, Y. F. Du, and M. H. Xu, "A mechanistic study of the effects of CO_2 on pyrrhotite oxidation," *Proceedings of the Combustion Institute*, vol. 36, no. 3, pp. 3925–3931, 2017.

[36] F. Q. Yang, Y. Z. Song, and W. F. Zhu, "Fractal characteristics of adsorption hole of FeS–FeS_2 compounds," *Journal of Fuzhou University (Natural Science Edition)*, vol. 47, no. 1, pp. 118–123, 2019.

[37] Y. Li, R. van Santen, and T. Weber, "High–temperature FeS–FeS_2 solid–state transitions: reactions of solid mackinawite with gaseous H_2S," *Journal of Solid State Chemistry*, vol. 181, no. 11, pp. 3151–3162, 2008.

[38] China Standards, *Iron Ores–Determination Of Total Iron content–Titanium(III) Chloride Reduction Potassium*

Dichromate Titration Methods (Routine Methods), State Bureau of Technical Supervision, Beijing, China, 2009.

[39] China Standards, *Methods for Chemical Analysis of bauxite – Part 17: Determination of Sulfur Content Direct Combustion–Iodometric Method*, National Development and Reform Commission, Beijing, China, 2007.

[40] F. Huang, S. Z. Xin, T. Mi, and L. Q. Zhang, "Study of pyrite transformation during coal samples heated in CO_2 atmosphere," *Fuel*, vol. 292, Article ID 120269, 2021.

[41] S. Hosseinzadeh, F. Norman, F. Verplaetsen, J. Berghmans, and E. Van den Bulck, "Minimum ignition energy of mixtures of combustible dusts," *Journal of Loss Prevention in the Process Industries*, vol. 36, pp. 92–97, 2015.

[42] E. K. Addai, D. Gabel, and U. Krause, "Experimental investigations of the minimum ignition energy and the minimum ignition temperature of inert and combustible dust cloud mixtures," *Journal of Hazardous Materials*, vol. 307, pp. 302–311, 2016.

[43] T. Kennedy and B. T. Sturman, "The oxidation of iron (II) sulphide," *Journal of Thermal Analysis*, vol. 8, no. 2, pp. 329–337, 1975.

[44] N. Belzile, Y. W. Chen, M. F. Cai, and Y. Li, "A review on pyrrhotite oxidation," *Journal of Geochemical Exploration*, vol. 84, no. 2, pp. 65–76, 2004.

[45] R. Soundararajan, P. R. Amyotte, and M. J. Pegg, "Explosibility hazard of iron sulphide dusts as a function of particle size," *Journal of Hazardous Materials*, vol. 51, no. 1–3, pp. 225–239, 1996.

[46] F. R. A. Jorgensen and F. J. Moyle, "Gas diffusion during the thermal analysis of pyrite," *Journal of Thermal Analysis*, vol. 31, no. 1, pp. 145–156, 1986.

[47] M. Labus, "Pyrite thermal decomposition in source rocks," *Fuel*, vol. 287, Article ID 119529, 2021.

[48] X. Li, Y. J. Shang, Z. L. Chen et al., "Study of spontaneous combustion mechanism and heat stability of sulfide minerals powder based on thermal analysis," *Powder Technology*, vol. 309, pp. 68–73, 2017.

[49] G. S. Li, H. W. Cheng, X. L. Xiong et al., "In-situ high temperature X–ray diffraction study on the phase transition process of polymetallic sulfide ore," in *Proceedings of the IOP Conference Series: Materials Science and Engineering*, vol. 191, no. 1, IOP Publishing, Bangkok, Thailand, March 2017.

[50] E. Müsellim, M. H. Tahir, M. S. Ahmad, and S. Ceylan, "Thermokinetic and TG/DSC–FTIR study of pea waste biomass pyrolysis," *Applied Thermal Engineering*, vol. 137, pp. 54–61, 2018.

[51] N. Supriya, K. B. Catherine, and R. Rajeev, "DSC–TG studies on kinetics of curing and thermal decomposition of epoxy-ether amine systems," *Journal of Thermal Analysis and Calorimetry*, vol. 112, no. 1, pp. 201–208, 2013.

[52] W. Z. Lv, D. X. Yu, J. Q. Wu, L. Zhang, and M. Xu, "The chemical role of CO_2 in pyrite thermal decomposition," *Proceedings of the Combustion Institute*, vol. 35, no. 3, pp. 3637–3644, 2015.

[53] C. S. Tian, Y. Z. Rao, G. Su, T. Huang, and C. R. Xiang, "The thermal decomposition behavior of pyrite-pyrrhotite mixtures in nitrogen atmosphere," *Journal of Chemistry*, vol. 2022, Article ID 8160007, 11 pages, 2022.

[54] L. Li, J. X. Wang, C. Q. Wu, and A. Ghahreman, "An environmentally friendly method for efficient atmospheric oxidation of pyrrhotite in arsenopyrite/pyrite calcine," *Chemical Engineering Journal Advances*, vol. 7, Article ID 100122, 2021.